pISSN 2384-1095
eISSN 2384-1109

iMRI 2021;25:252-265

https://doi.org/10.13104/imri.2021.25.4.252

iMRI
Investigative Magnetic Resonance Imaging

Fast Real-Time Cardiac MRI: a Review of Current Techniques and Future Directions

Xiaoqing Wang[1,3], Martin Uecker[1,2,3], Li Feng[4]

[1]Institute for Diagnostic and Interventional Radiology, University Medical Center Göttingen, Göttingen, Germany
[2]Institute of Biomedical Imaging, Graz University of Technology, Graz, Austria
[3]German Centre for Cardiovascular Research (DZHK), Partner Site Göttingen, Göttingen, Germany
[4]Biomedical Engineering and Imaging Institute and Department of Radiology, Icahn School of Medicine at Mount Sinai, New York, NY, USA

Review Article

Received: October 8, 2021
Revised: November 9, 2021
Accepted: November 12, 2021

Correspondence to:
Xiaoqing Wang, Ph.D.
Institute of Diagnostic and Interventional Radiology, University Medical Center, Robert-Koch-Str, 40 Göttingen, Germany.
Tel. +49-551-39-63963
Fax. +49-551-39-63963
E-mail: xiaoqing.wang@med.uni-goettingen.de

Cardiac magnetic resonance imaging (MRI) serves as a clinical gold-standard non-invasive imaging technique for the assessment of global and regional cardiac function. Conventional cardiac MRI is limited by the long acquisition time, the need for ECG gating and/or long breathhold, and insufficient spatiotemporal resolution. Real-time cardiac cine MRI refers to high spatiotemporal cardiac imaging using data acquired continuously without synchronization or binning, and therefore of potential interest in overcoming the limitations of conventional cardiac MRI. Novel acquisition and reconstruction techniques must be employed to facilitate real-time cardiac MRI. The goal of this study is to discuss methods that have been developed for real-time cardiac MRI. In particular, we classified existing techniques into two categories based on the use of non-iterative and iterative reconstruction. In addition, we present several research trends in this direction, including deep learning-based image reconstruction and other advanced real-time cardiac MRI strategies that reconstruct images acquired from real-time free-breathing techniques.

Keywords: Real-time cardiac MRI; GRAPPA; Iterative SENSE; NLINV; Non-Cartesian; Motion-resolved image reconstruction

INTRODUCTION

Cardiac magnetic resonance imaging (MRI) is a valuable and powerful non-invasive imaging modality for evaluating the cardiovascular system. In particular, cardiac cine MRI is currently considered as the clinical standard for assessing global cardiac function and is increasingly used to measure regional cardiac function (1). To evaluate the rapid movements of myocardial wall and valves, conventional cardiac cine MRI acquisition relies on ECG gating (2) to generate images at different cardiac phases and requires breath holding to avoid respiratory motion artifacts. Using ECG-gated and breathhold acquisition techniques, data at the same cardiac phase but different cardiac cycles can be combined together to generate high-quality images with sufficient spatial and temporal resolution within a single breathhold. However, the use of standard ECG-gated and breathhold cardiac cine MRI is limited by two major challenges clinically. First,

for patients with reduced breathholding capacity, cardiac cine images can be substantially degraded by respiration-induced artifacts. Second, for patients with arrhythmias, ECG gating and data synchronization from different cardiac cycles is less reliable, resulting in motion artifacts such as ghosting and/or blurring.

Alternatively, cardiac cine MR images can also be acquired continuously and with cardiac phases of each heartbeat reconstructed separately without combining data from different heartbeats into the same image (3, 4). ECG gating is then not needed. The reconstructed images represent the true physiological cardiac movement in real time. This technique, known as real-time cardiac MRI, has attracted substantial attention in the field due to its improved robustness. Unfortunately, acquiring multiple cardiac phases (e.g., 15-25) within one cardiac cycle is very challenging due to the slow imaging speed of MRI, which limits the spatiotemporal resolution compared with the conventional ECG-gated and breathhold counterpart. To achieve the desired spatiotemporal resolution, highly-accelerated data acquisition is needed, which requires special strategies to reconstruct the undersampled cardiac MRI data.

This review article aims to provide a brief overview of image acquisition and reconstruction methods that have been proposed for real-time cardiac MRI. We classified the existing real-time cardiac cine methods into two categories based on the need for iterative reconstruction. Finally, we discuss current research trends in this direction, including deep learning-based image reconstruction and other more advanced real-time cardiac MRI strategies. Note that the terminology "real-time" is often used elsewhere in a stricter sense, which also requires real-time image reconstruction available for immediate use with low latency (5). We will focus on the more general concept in this review.

Accelerated Real-Time Cardiac MRI Using Non-Iterative Reconstruction Techniques

Parallel Imaging and k-t Techniques

Parallel imaging (PI) has been developed for accelerating MRI acquisition (6-8) more than two decades ago. Based on complementary information acquired from multiple receiver coil arrays, parallel imaging techniques, such as SENSitivity Encoding (SENSE) and GeneRalized Autocalibrating Partial Parallel Acquisition (GRAPPA), normally achieve an acceleration factor of 2-4. The earliest application of SENSE in real-time cardiac MRI has been reported (9) using an acceleration factor of 3.2. Conventional PI needs to determine the prior information needed for reconstruction, namely, the coil sensitivity maps for SENSE (7) or the reconstruction weights for GRAPPA (8). Both are usually obtained from a low-resolution calibration scan. The temporal SENSE (TSENSE) (10) and GRAPPA (TGRAPPA) (11) techniques avoid the above calibration acquisition steps by applying a sliding window reconstruction to the dynamic k-space to obtain a set of fully sampled high-resolution images (but with a lower temporal resolution). Following estimation of the prior information for parallel imaging from these high-resolution images, each time frame can then be separately reconstructed with either SENSE or GRAPPA.

Methods that jointly utilize spatiotemporal redundancy have also been developed. These methods are typically referred to as "k-t techniques", which can also be further combined with parallel imaging. The representative non-iterative k-t techniques include UNFOLD (12), k-t BLAST (13), k-t PCA (14) and others (15, 16). K-t techniques usually convert the undersampled data from k-t space to x-f space, where x and f represent the spatial position and temporal frequency, respectively, eliminating the aliasing artifacts in the x-f space and transforming the data into dynamic images. They can be further combined with parallel imaging methods, such as the k-t SENSE (13) and k-t GRAPPA (17) techniques. Although an acceleration factor of around 8 can be achieved using the combined k-t technique with parallel imaging, they also introduce temporal blurring at high acceleration rates. A comprehensive review of the k-t techniques (including the iterative ones) has been published (18).

However, non-Cartesian trajectories, such as radial (19) or spiral (20) sampling, facilitate a more efficient coverage of k-space, and are more robust to motion artifacts. In the following section, we will introduce the combination of non-Cartesian trajectories with GRAPPA for real-time cardiac MRI.

Real-Time Cardiac MRI via Through-Time Non-Cartesian GRAPPA

GRAPPA is an auto-calibrating coil-by-coil reconstruction method used in parallel imaging. Basically, GRAPPA is used to estimate the missing k-space as an interpolation, i.e., the missing k-space data (the target points) can be determined by a weighted linear combination of acquired k-space points (neighborhood) from all coils (21).

We formulated the estimated target information using a notation reported previously (22):

$$\hat{s}_{targ,j}(k_x, k_y + \delta k_y) = \sum_{i=1}^{N} \sum_{\tau x} \sum_{\tau y} n(i, j, \tau_x, \tau_y) \cdot S_{src,i}(k_x + \tau_x, k_y + \tau_y) \quad [1],$$

where $\hat{s}_{targ,j}(k_x, k_y+\delta k_y)$ is the target k-space data to be estimated in the jth coil and at location $(k_x, k_y+\delta k_y)$, $\hat{s}_{targ,j}(k_x+\tau_x, k_y+\tau_x)$ denotes a source point in the kernel from coil i, whereas τ_x and τ_y indicate the positions in the kernel, and $n(i,j,\tau_x,\tau_y)$ represents the value of the GRAPPA weight set for the proper target and source coils and position.

The above GRAPPA weight is estimated from the additional fully-sampled auto-calibration k-space lines (known as auto-calibration signals, ACS). In ACS, both the source and target points are known:

$$s_{targ,j}(k_x,k_y+\delta k_y) = \sum_{i=1}^{N} \sum_{\tau x} \sum_{\tau y} n(i, j, \tau_x, \tau_y) \cdot S_{src,i}(k_x + \tau_x, k_y + \tau_y) \quad [2],$$

where $s_{targ,j}$ is the known target k-space value. All the source and target points in the ACS are then used to calculate the GRAPPA weight and the number of kernels should be large enough to ensure the accuracy of the calibration equation is well determined.

For Cartesian GRAPPA with regular undersampling, a single kernel can be used and the kernel weights can be estimated from the ACS data. However, for undersampled non-Cartesian imaging, such as radial GRAPPA, multiple kernels are needed due to the variation in the degree and direction of undersampling (22). In this case, fully sampled k-space instead of ACS data are needed for calibration. As shown in Figure 1a, the fully-sampled k-space is divided into multiple k-space segments and the set of GRAPPA weights is calculated for each segment individually. This is so called segmented k-space calibration. To allow for accurate determination of the weights, a small segment size is needed, suggesting the need for additional sets of GRAPPA weights (unknowns) estimated through the k-space, resulting in inaccurate estimation. To improve the conditioning, a through-time GRAPPA calibration is used in which multiple fully-sampled k-space data along time are acquired and utilized to determine the GRAPPA weights for each segment. Figure 1b presents the basic idea of the above calibration. Note that the fully-sampled k-space requires the same trajectory and should specifically cover the radial angles for undersampled acquisitions. When only the through-time calibration is used, the number of frames can be up to 350 to 400, i.e., more than 1 min for an in-plane resolution of 2.34 × 2.34 mm^2 for cardiac imaging (22). To reduce the calibration time/frames, a hybrid segmented (through k-space) and through-time calibration is employed for real-time cardiac imaging. Figure 2 illustrates sample real-time cardiac images reconstructed from data containing 14 radial projections/frame with a spatial resolution of 2.34 mm^2 and a temporal resolution of

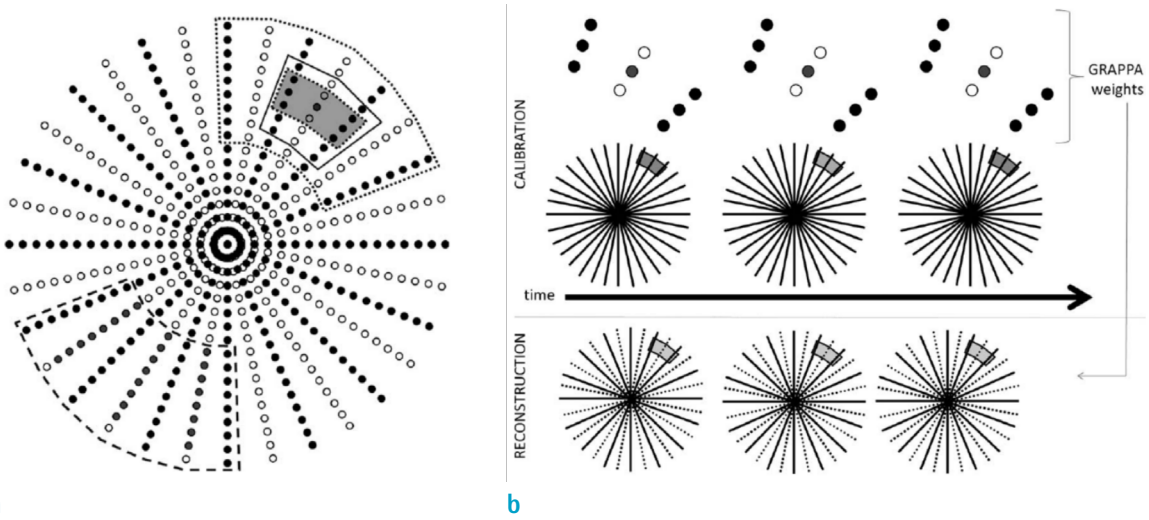

Fig. 1. (a) Segmented (through k-space) GRAPPA calibration (b) Through-time GRAPPA calibration. Note that all the fully-sampled k-space contains the same trajectory in (b) and covers the radial angles for undersampled acquisitions. A hybrid version of both calibration strategies is utilized in real-time cardiac imaging. Images were obtained from Figs. 1 and 2 in Seiberlich et al. Magn Reson Med 2011;65:492-505, and reproduced with permission.

Fig. 2. Sample images reconstructed from data containing 12 projections/frame with a spatial resolution of 1.56 mm^2 and a temporal resolution of 36 msec/frame. Hybrid radial GRAPPA was used with 75 calibration frames (requiring a calibration scan time of 32.4 sec), and 8 × 1 sized k-space segments. Images were sourced from Fig. 10 in Seiberlich et al. Magn Reson Med 2011;65:492-505, and reproduced with permission.

40 ms/frame. The calibration parameters included 25 frames (requiring a scan time of 9.94s), and k-space segments with a size of 8 × 4 (read × projection) .

A spiral version of through-time GRAPPA has also been proposed for real-time cardiac imaging (23). Spiral trajectory covers the k-space more efficiently than a radial scan. Thus, it can achieve a higher spatiotemporal resolution than radial sampling within the same amount of time. A temporal resolution of 18 ms/image has been demonstrated for real-time cardiac imaging (23). Compared with radial imaging, spiral imaging may introduce off-resonance artifacts due to the use of a long readout. Moreover, it is difficult to perform a thorough k-space calibration as the spiral arms do not "line up" like the radial trajectories (23). To facilitate accurate calibration, additional through-time acquisitions of the fully-sampled dataset are then needed.

Accelerated Real-Time Cardiac MRI Using Iterative Reconstruction Techniques

Non-Cartesian Iterative SENSE

Alternatively, the MR signal equation for parallel imaging can be interpreted as a nonlinear equation with an operator E mapping both the image content m and coil sensitivity maps $(c_1,\cdots c_N)^T$ to the measured data y:

$$y=E(x), with\ x=\begin{pmatrix} m \\ c_1 \\ \vdots \\ c_N \end{pmatrix} and\ E{:}x \rightarrow \begin{pmatrix} PF\,(m \cdot c_1) \\ \vdots \\ PF\,(m \cdot c_N) \end{pmatrix} \quad [3],$$

where y is the k-space data, F represents the Fourier transform, P denotes sampling pattern, c_i indicates the ith coil sensitivity map, and m refers to the desired image to be reconstructed. Since both image content and coil sensitivity maps are unknown, parallel imaging is intrinsically a nonlinear (bi-linear) inverse problem. The SENSE method reduces the nonlinear challenge to a linear problem by first estimating coil sensitivities using calibration data and then reconstructing the image content in a linear manner. Thus, the two-step autocalibrating SENSE method involves 1) determination of coil sensitivity maps from ACS lines, followed by 2) linear reconstruction of image content. Several methods are available for the calibration of coil sensitivity maps. Two representative techniques include the adaptive method (24) and ESPiRiT (21). Following coil calibration, the reconstruction problem can be formulated as:

$$\hat{m} = \underset{m}{argmin} ||y - E(m)||_2^2 + \lambda \cdot R(m) \quad [4],$$

where $R(\cdot)$ defines the regularization term with λ the regularization parameter. The above model allows an easier extension to non-Cartesian trajectories (25) via adaption of the sampling pattern P in equation [3]. In the original implementation, $R(\cdot)$ was selected as the Tikhonov (L2) regularization to stabilize the reconstruction (i.e., to reduce noise):

$$R(m) = ||m||_2^2 \quad [5]$$

The above equation [4] can then be effectively solved using the conjugate gradient algorithm. Figure 3 illustrates real-time cardiac imaging using the SENSE method to achieve a temporal resolution of 56 ms with a spiral trajectory using four coils.

Regularized Nonlinear Inversion

An extension of the SENSE method is to jointly estimate both image content and coil sensitivity from the acquired data without any calibration step. This category includes mainly two methods. First, the joint SENSE (JSENSE) (26) technique, which formulates image reconstruction and coil sensitivity maps as an alternative minimization problem,

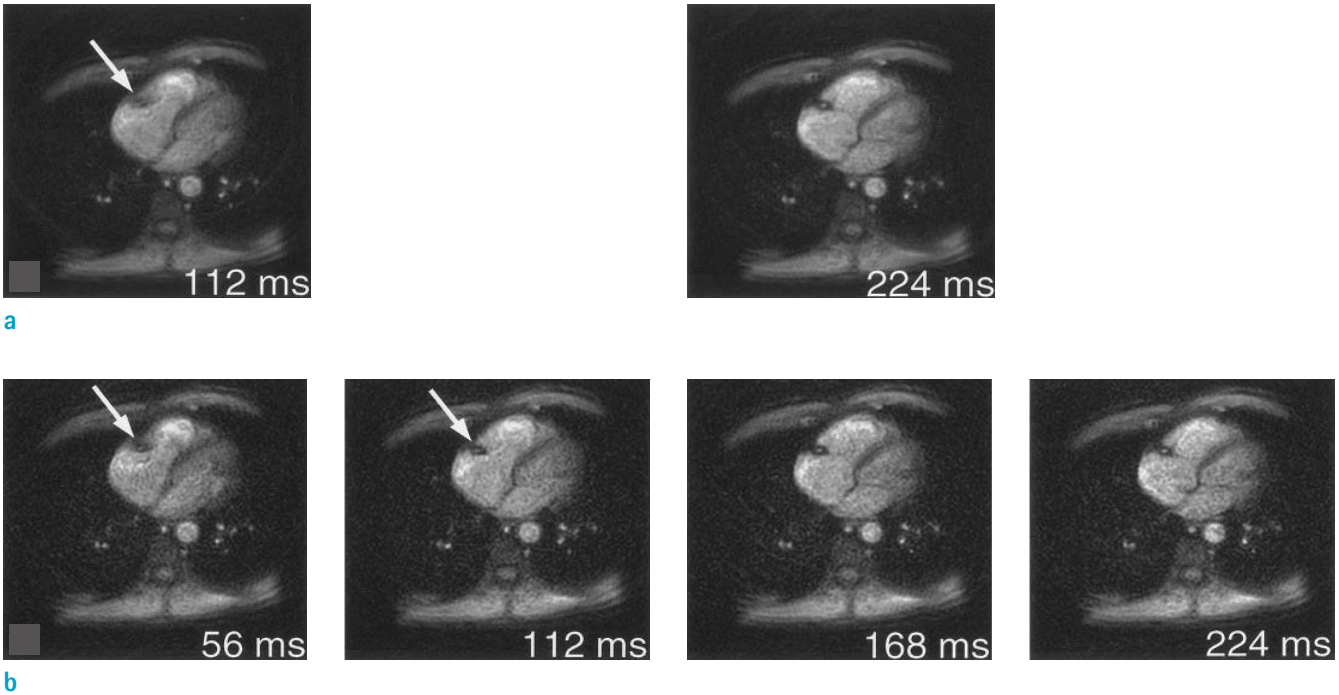

Fig. 3. Real-time cardiac imaging. Sensitivity-encoded heart imaging with four coils, using a real-time spiral protocol. (a) Conventional reconstruction from fully-Fourier-encoded data obtained with four successive spiral interleaves. (b) Images obtained from the same data via sensitivity-based reconstruction using only two successive interleaves for each image. Thus, the scan time per image was reduced from 112 ms to 56 ms. Images were obtained from Fig. 6 in Pruessmann et al. Magn Reson Med 2001;46:638-651, and reproduced with permission from the journal.

i.e., the optimization of image and coil sensitivity maps was performed in an alternative manner, resulting in a linear inverse relationship at each iteration step. Moreover, JSENSE employs a polynomial model to smoothen the coil sensitivity maps. Second, the regularized nonlinear inversion (NLINV) (27) method is used to formulate the reconstruction of both image and coil sensitivity maps as a more general nonlinear inverse problem using a Newtonian method. The cost function for NLINV can be written as:

$$\hat{x} = \underset{x}{argmin} ||y - E(x)||_2^2 + \lambda \cdot R(x) \quad [6]$$

with the unknown x containing both image and coil sensitivity maps. The above nonlinear equation is then solved by the iteratively regularized Gauss-Newton method (IRGNM) (28, 29), which linearizes and solves the nonlinear equation at each Gauss-Newton step, i.e.,

$$\hat{x}_{k+1} = \underset{x}{argmin} ||y - (DE(x_k)(x-x_k) + E(x_k))_2^2 + \lambda_k \cdot R(x) \quad [7],$$

where $DE(x_k)$ is the Fréchet derivative of E at the current estimate x_k and the regularization parameter λ_k is reduced in each Gauss-Newton step, i.e., $\lambda_k = \lambda_0 \cdot q^k$ with $\lambda_0 = 1$ and $q \in (0,1)$. Notably, equation [3] represents a nonlinear problem that is highly underestimated even for the fully sampled case. A direct application of IRGNM to the above nonlinear problem would therefore result in an unrealistic solution. To overcome this problem, NLINV introduces the Sobolev regularization to penalize the high frequency of the coil sensitivities (enforce smoothness), i.e.,

$$R(c_i) = ||(1 + s||\vec{k}||^2)^{l/2} Fc_i||^2 \quad [8],$$

with $||\vec{k}||$ defining the distance to the k-space center, while s and l represent positive constants. A reasonable value for s and l would be s = 400 mm^2 and l = 16. Further, the L2 regularization is applied to both image and coil sensitivity maps. For real-time applications, the L2 regularization also incorporates the difference between the current image frame with respect to a weighted previous frame, i.e.,

$$R(x) = ||x - w \cdot x_{t-1}||_2^2 \quad [9],$$

with w denoting the weighting parameter, which is often in the range of (0.5, 1.0) (30) and x_{t-1} represents the image from a previous frame. Equation [7] can be analyzed and rewritten as:

$$\hat{x}_{k+1} = (DE^H(x_k)DE(x_k) + \lambda_k I)^{-1} (DE^H(x_k)(y - E(x_k) + DE(x_k)x_k) + \lambda_k \cdot w \cdot x_{t-1}) \quad [10],$$

with I denoting the identity matrix. Equation [10] can be effectively solved using the conjugate gradient algorithm as well. When extending from Cartesian to non-Cartesian trajectories, NLINV uses the convolution-based gridding technique (31) for efficient computation of graphical processing units (GPUs) (32).

Figure 4 illustrates real-time cardiac MR imaging using undersampled radial FLASH and NLINV at the middle short-axis of the left ventricle (33). The data were acquired continuously at a spatial resolution of 1.5 × 1.5 × 8 mm^3 and with a TR/TE value of 2.2/1.4 ms, flip angle 8°, and 15 spokes per frame (temporal resolution 33 ms).

Compared with SENSE-based approach, the NLINV-based method avoids calibration errors by jointly estimating both images and coil sensitivity maps based on similar data. This approach enhances the value of NLINV in real-time applications, especially for acquisitions during free breathing, dynamic contrast changes or rapid changes in the imaging plane, such as interactive cardiac MRI (34, 35). A recent clinical study of patients with heart failure manifesting preserved ejection fraction (HFpEF)-Stress suggested that the NLINV-based real-time CMR technique allows highly accurate identification of HFpEF during physiological exercise and may qualify as a suitable noninvasive diagnostic alternative to invasive catheterization (36). Moreover, the efficient implementation of NLINV with multiple GPUs (37) not only enables the real-time acquisition of MRI data but also allows real-time image reconstruction, i.e., reconstructed NLINV images are available for immediate use with low latency (5). In addition, the general framework in the forward model also enables the extension of NLINV for more advanced nonlinear reconstruction incorporating MR physical models in the forward model for efficient quantitative imaging (38-42). Real-time MRI based on the NLINV framework has been reviewed recently (3).

Compressed Sensing

Compressed sensing (CS) (43, 44) is a powerful technique for image acceleration and has been widely used in both static and dynamic MR imaging (45-48). The success of CS MRI relies on three basic components: 1) sparsity or transform sparsity of the target image; 2) incoherent sampling where the incoherence is assessed based on

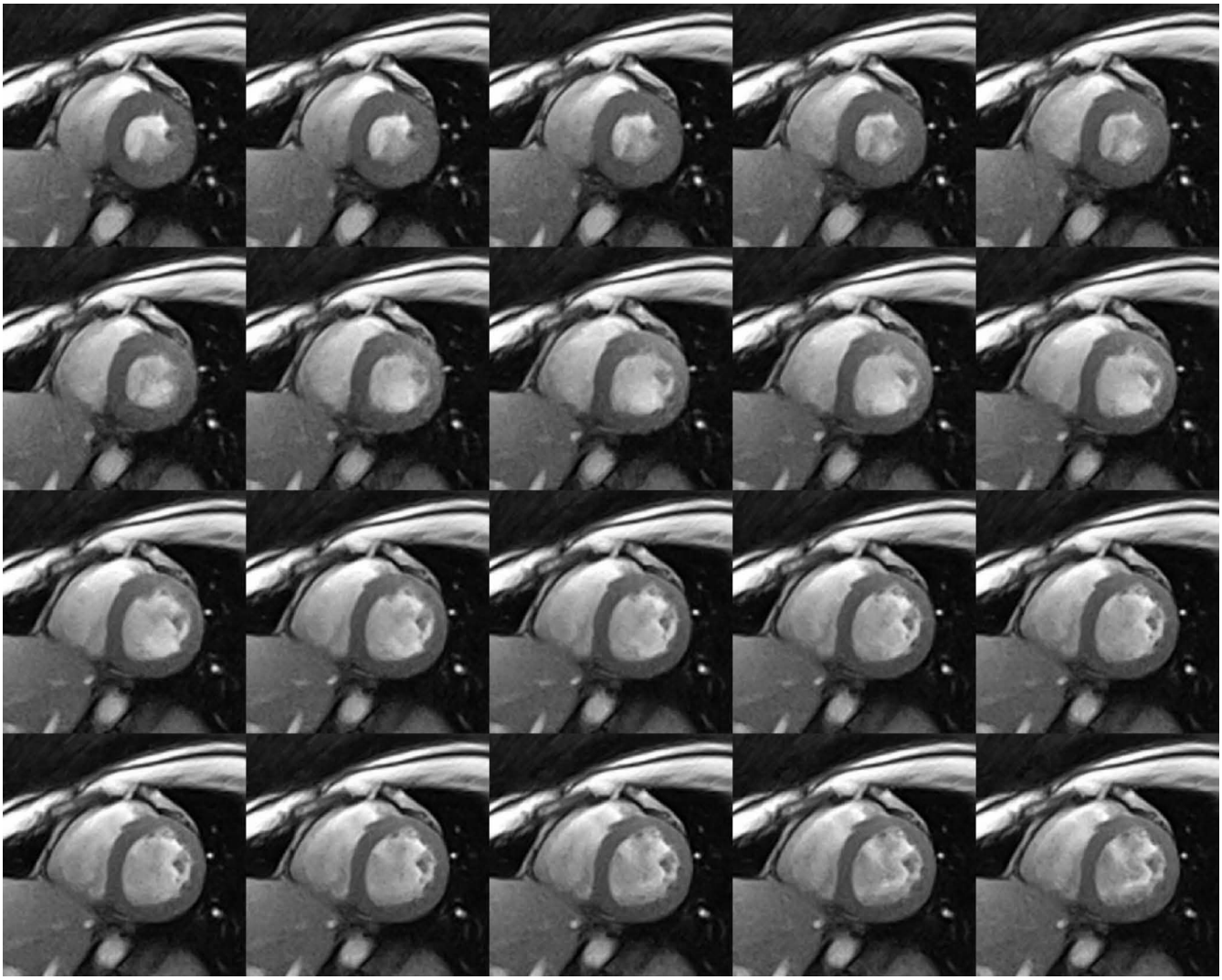

Fig. 4. Real-time radial FLASH CMR at 1.5 mm spatial resolution and 33 ms temporal resolution. The data was acquired continuously with TR/TE = 2.2/1.4 ms, flip angle 8°, 15 radial spokes per frame. Images were obtained from Fig. 7 in Zhang et al. J Cardiovasc Magn Reson 2010;12:39, and reproduced with permission from the journal.

sampling and sparsity; and 3) a nonlinear reconstruction algorithm to solve the regularized inverse problem.

In practice, an MR image is not necessarily sparse by itself. Images need to be subjected to specific transformations such as finite differences or wavelets to generate a sparse representation. For dynamic imaging, the temporal sparsity can be additionally exploited. In contrast to regular undersampling, incoherent undersampling generates noise-like incoherent artifacts, which can then be iteratively reduced in a nonlinear reconstruction step. For Cartesian 2D imaging, incoherence can be achieved via sampling pattern design along the phase encoding direction. However, non-Cartesian trajectories such as radial and spiral sampling exhibit intrinsic incoherence greater than the Cartesian type. Furthermore, higher incoherence can be achieved in 3D or dynamic imaging as the additional dimension provides an extra degree of freedom for designing sampling patterns.

CS has been combined with the aforementioned parallel imaging (46, 49, 50) as well as k-t techniques for accelerated imaging (48-55). In the following, we will focus on the k-t SPARSE-SENSE method (56), which belongs to iterative k-t techniques, and has been demonstrated in real-time cardiac MRI.

K-t SPARSE-SENSE exhibits a pseudo-random variable-density trajectory and varies the sampling pattern along time to achieve incoherence in k-t space. A sampling example is presented in Figure 5. Similar to the k-t techniques introduced before, the k-t SPARSE-SENSE

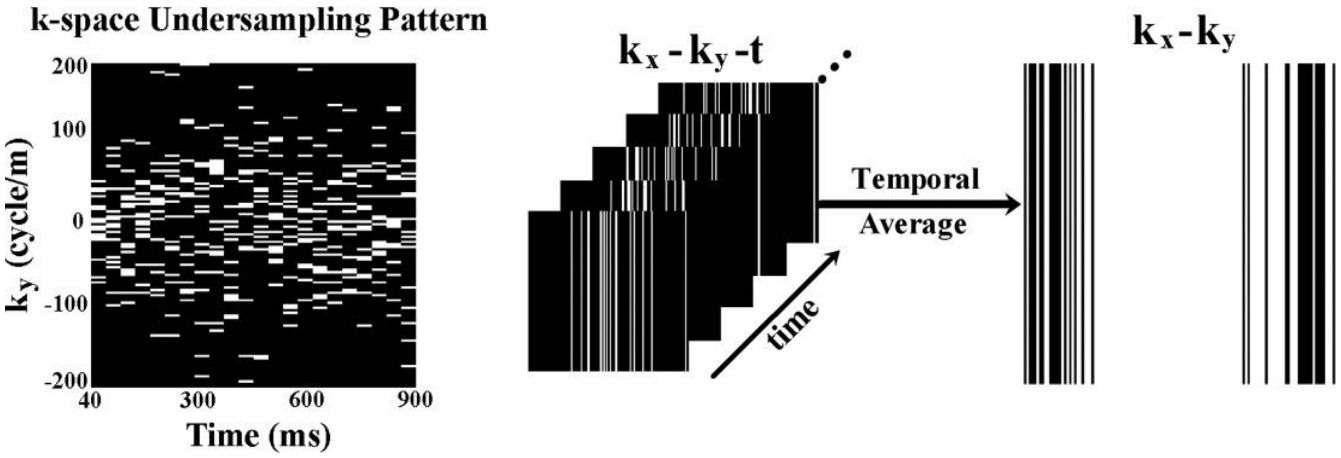

Fig. 5. (a) Eight-fold accelerated ky-t sampling pattern variation with time. (b) A schematic representation of the average kx-ky-t sampling pattern over time resulting in kx-ky sampling pattern, which represents the sampling used to perform self-calibration of coil sensitivities (see Fig. 6 for cross-reference). White lines represent acquired samples. Images were obtained from Fig. 1 in Feng et al. Magn Reson Med 2013;70:64-74, and reproduced with permission from the journal.

approach also converts data from k-t space to x-f space. Here f can be an arbitrary sparsity transform, such as temporal fast Fourier transform (FFT), temporal principal component analysis (PCA) or temporal total variation (TV). In the x-f space, the images lie in compact regions while the incoherent artifacts are randomly distributed. As a result, the reconstruction can separate the true image and the artifacts iteratively (18). Mathematically, with the series of dynamic images unknown, the reconstruction problem can be written as:

$$\hat{m} = \underset{m}{argmin} ||y - E(m)||_2^2 + \lambda \cdot R(m) \quad [11],$$

with m = $(m1,\cdots m_n)^T$ representing the image series for reconstruction. The regularization term is derived using the formula below:

$$R(m) = ||T(m)||_1 + \alpha \cdot ||Wm||_1 \quad [12]$$

Here, *T* is a temporal sparsity transform, which may be a temporal PCA, temporal FFT or temporal *TV*, W denotes the spatial wavelet transform and α is the weighting parameter balancing the effects of the two regularization terms. Various techniques can be used to solve the above sparsity-constrained inverse problem, i.e., equation [11]. Representative methods include nonlinear conjugate gradient (57), (Fast) iterative shrinkage-thresholding algorithm (58, 59) and alternating direction method of multipliers (ADMM) (60). Figure 6 illustrates end-diastolic and end-systolic events at multiple cardiac phases with comparable image quality using breathhold cine MRI and real-time cine MRI with k-t SPARSE-SENSE.

In contrast to the aforementioned iterative methods used to reconstruct a single image at one time, the k-t SPARSE-SENSE can be used to estimate the entire image series as an inverse problem based on thew spatiotemporal sparsity in the additional time dimension. However, SENSE/NLINV-based approach can be used in real-time interactive applications as it only needs data acquired before the current frame (causal) without waiting for subsequent data acquisition.

Aside from the combined temporal sparsity and the spatial L1-Wavelet regularization demonstrated in equation [12], other sparsity transforms such as 3D Haar wavelets (61) have also been utilized to exploit the spatial-temporal sparsity in the 2D+t cardiac data. More advanced regularization, such as non-local patch-based (62) or dictionary-based (63-65) regularization may also be used for real-time cardiac imaging.

Other CS-based imaging technique for real-time cardiac MRI is the low-rank (66, 67) or joint low-rank and sparsity constraint (68, 69)-based approaches. This type of method is based on the theoretical framework considering the k-t space as partially separative along the spatial and temporal dimensions (70), resulting in a rank-deficient matrix. Therefore, reconstruction of the dynamic data can be formulated as a low-rank matrix recovery problem, which can be solved using low-rank recovery techniques. The k-t

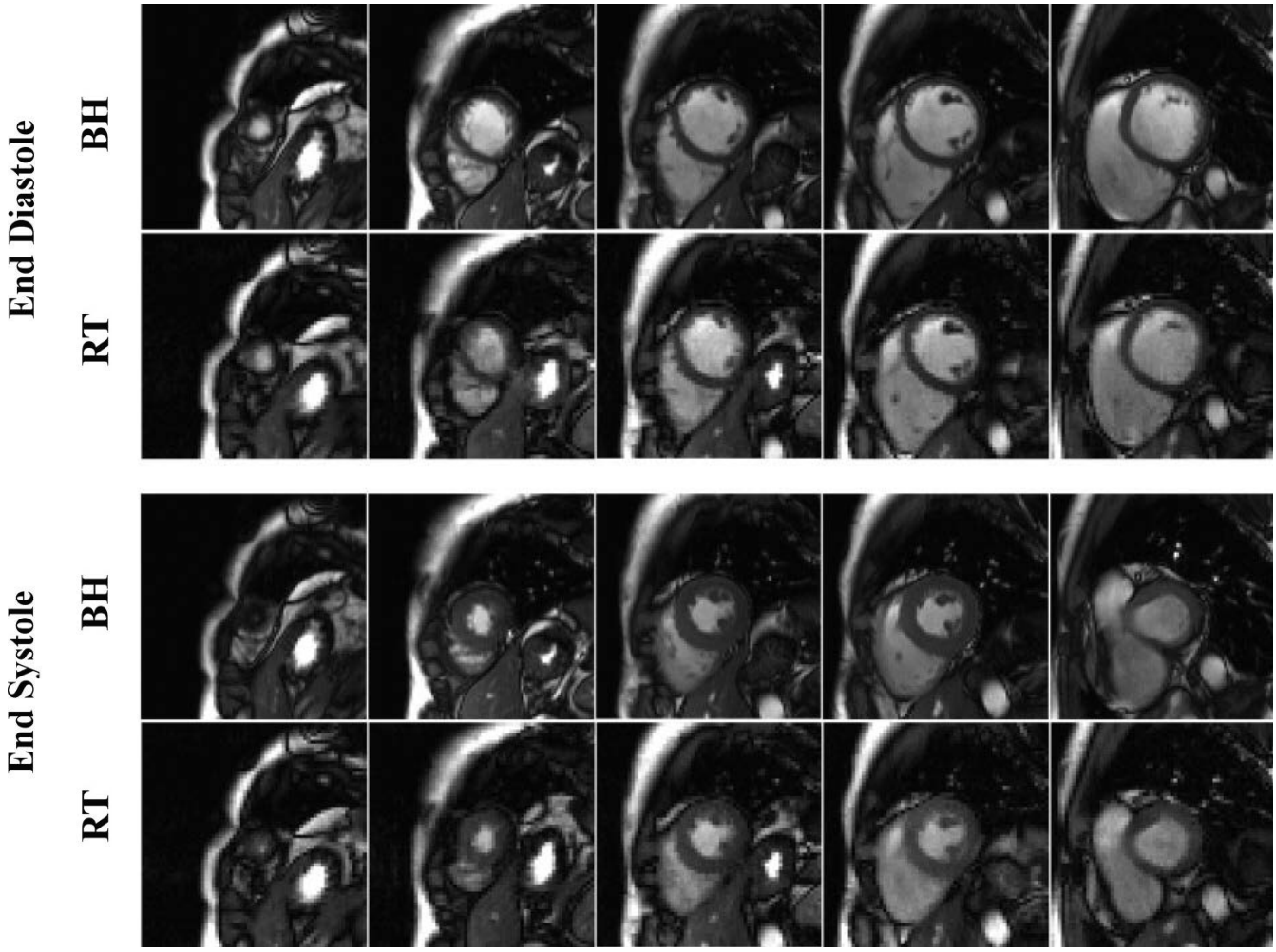

Fig. 6. (Rows 1, 2) End-diastolic and (rows 3, 4) end-systolic images at multiple cardiac phases comparing (rows 1 and 3) breathhold cine MRI and (rows 2 and 4) real-time MRI. Both image sets were acquired from a 29-year-old (male) healthy subject. Real-time MRI yielded average scores of 3.25, 4.3, 2.6, and 2.4 for image quality, temporal fidelity, artifact, and noise level, respectively, whereas the corresponding scores for breathhold cine MRI were 4.9, 5, 1.1, and 1.1, respectively. BH = breathhold; RT = real-time. The breathhold cine MR images exhibited higher spatial resolution than real-time MR images (1.6 mm vs. 2.3 mm, respectively). Images were sourced from Fig. 7 in Feng et al. Magn Reson Med 2013;70:64-74, and reproduced with permission from the journal.

signal can be arranged in a matrix form, where the rows correspond to the k-space points and the columns represent the time samples as in the partially separative function (PSF) model (70):

$$\Gamma = \begin{pmatrix} y(k_1, t_1) & \cdots & y(k_1, t_T) \\ \vdots & \ddots & \vdots \\ y(k_M, t_1) & \cdots & y(k_M, t_T) \end{pmatrix}$$

with M the number of k-space points and T the number of time points. Due to the strong spatial-temporal correlations, the above matrix has a low-rank property. i.e.,

$$rank(\Gamma) \leq L,$$

with a small L value, suggesting fewer degrees of freedom than the total number of elements in Γ. In addition to the low rank, sparsity constraints along both spatial and temporal dimensions can be further exploited (68), resulting in the following optimization problem:

$$\hat{m} = \underset{m}{argmin} ||y - E(m)||_2^2 + \mu \cdot ||\Gamma||_* + \lambda \cdot R(m) \qquad [13],$$

where $||\cdot||_*$ is the nuclear norm and $R(\cdot)$ represents spatial and temporal regularization. The above optimization

problem can be solved using a variable splitting algorithm proposed previously (68). The joint low-rank and sparsity constraints may lead to a higher acceleration factor than the low-rank constraints alone in real-time cardiac imaging (68, 69).

Future Directions

The focus of the present review is mainly on fast imaging methods designed to reconstruct real-time cardiac cine images without synchronizing or exploiting multi-heartbeat information. Since commonly used cardiac cine MRI sequences usually need time to achieve a steady state, practical real-time cardiac MRI acquisition is typically performed for two heartbeats, with the first heartbeat used to achieve a steady state and the second heartbeat utilized for data acquisition. Following data acquisition, the first heart beat can simply be discarded and a dynamic cardiac cine image series can be reconstructed from the second heartbeat. In this acquisition scheme, the respiratory motion need not be considered given the short acquisition time. In addition, several advanced methods for fast cardiac MRI are available to reconstruct cardiac cine images using data derived from multiple cardiac cycles. Strictly speaking, these methods do not belong to real-time cardiac MRI because they combine data from multiple cycles. However, they are briefly discussed to provide a future research direction and trend.

First, motion-correction techniques (71-75) consider motion in the reconstruction of cardiac cine MRI using data from more than one cardiac cycle. In this method, the respiratory motion is first estimated using images reconstructed with a moderate temporal window, e.g., a window size with a RR interval. Subsequently, the estimated motion field is incorporated into the forward model (equation [3]) in the iterative image reconstruction. As an example, the combination of a motion-correction technique using optical flow with the SPIRiT non-linear reconstruction using temporal regularization was used for multiple heartbeat reconstruction in cardiac cine imaging with high spatial (1.3-1.8 × 1.8-2.1 mm^2) and temporal resolution (retrospectively gated, 30 cardiac phases, temporal resolution 34.3 ± 9.1 ms) (73).

Second, multi-dimensional methods which combine non-Cartesian sampling, self-gating and motion-resolved image reconstruction have gained a lot of interest recently (76-83). The representative techniques include golden-angle radial sparse parallel (GRASP) (76), XD-GRASP (77), SmooThness Regularization on Manifolds (SToRM) (78) and MR multitasking (79-81). GRASP is an extension of k-t SPARSE-SENSE to non-Cartesian trajectories, in particular gold-angle radial sampling (84). XD-GRASP further extends GRASP to multidimensional reconstruction with an extra-respiratory dimension to avoid explicit motion correction. Following self-gating (85) based on radial k-space center signals and sorting the data into multiple cardiac and respiratory phases, XD-GRASP imposes additional temporal sparsity constraints along both respiratory and cardiac dimensions to improve the reconstruction performance. This method can be used for cardiac imaging at a spatial resolution of 2 × 2 mm^2 and a temporal resolution of 45 ms via continuous radial acquisitions. The SToRM technique models the dynamic image frames as points on a smooth and low dimensional non-linear manifold considering each image frame in the dataset as a non-linear function based on a few physiological parameters (e.g., cardiac and respiratory phase in real-time cardiac cine). In contrast to the temporal regularization used in XD-GRASP, the SToRM employs a manifold smoothness regularization to reconstruct the entire dynamic images. MR multitasking is another type of multi-dimensional approach, which incorporates not only physiological parameters such as respiratory and cardiac motion, but also other dynamic physical parameters (T1, T2 relaxation) into the reconstruction. Since this additional dimension is also distinct, the new high-dimensional data are ranked lower to facilitate the reconstruction of large images via a low-rank tensor-based approach. This technique enables time-resolved cardiac T1, T2, and ECV mapping without the use of ECG triggering or breathholds. Notably, all the above methods rely on accurate and robust motion signal estimation, which can be achieved by applying band-pass filter (85), and techniques such as PCA (77), adapted singular spectrum analysis (SSA) (86) to reduce dimensionality of auto-calibration (AC) data from certain receiver coils.

Third, deep learning (DL)-based approaches (87-96) represent a new trend in accelerated MR imaging in which the handcrafted sparsity transform (TV, Wavelet) is replaced by convolutional neural network (CNNs), where the model parameters can be learned from reference training data. Moreover, the iterative algorithms used in CS-like reconstruction can be expressed as a neural network (92), i.e., each layer in the network represents an iteration step of an iterative algorithm (88). Thus, the DL reconstruction can be performed by updating the network parameters in each iteration step. The main advantages of DL-based approaches

are two-fold. First, the learned regularizer is tailored for a specific task and is therefore expected to effectively eliminate residual artifacts compared with a handcrafted regularizer. Second, once the network has been trained and the weights are estimated, effective reconstruction can enhance the computational speed compared with regularized reconstructions (92). Application of DL to accelerated cardiac imaging was reported by Schlemper et al. (89), who proposed a deep cascade of CNN to learn spatiotemporal correlations by combining convolution and data-sharing approaches. Their network outperforms the CS-like approaches and resulted in a 9-fold acceleration using Cartesian sampling. Interestingly, a 3D (2D plus time) residual U-Net was trained to eliminate the artifacts (96). An acceleration factor of 13 was achieved using a tiny golden-angle radial bSSFP acquisition (97).

Summary

In summary, this brief review introduces two main categories of reconstruction methodology developed in the last two decades to accelerate real-time cardiac cine MRI. The first category entails non-iterative imaging reconstruction using linear reconstruction algorithms generally. In particular, the more recent through-time GRAPPA approach has attracted substantial attention. Despite the need for a relatively long calibration acquisition, the combination of non-Cartesian sampling and GRAPPA yielded reasonable spatiotemporal resolution in an acceptable time for real-time cardiac imaging. The second category involves iterative reconstruction approaches. Starting from non-Cartesian iterative SENSE, which is one of the earliest applications of parallel imaging techniques to real-time cardiac cine MRI, we proceeded to the NLINV method, which can be considered as an extension of iterative SENSE by jointly estimating both image content and coil sensitivity maps, and regularization to adjust for the differences between the current image frame to the previous one, facilitating real-time applications. NLINV enables applications with changing coil sensitivity maps due to variation in breathing or contrast. NLINV can also be used to reconstruct images in real time for interactive MRI applications. Furthermore, we illustrated the role of CS in accelerating real-time cardiac imaging. Instead of reconstructing a single image, one of the CS-based techniques known as k-t SPARSE-SENSE can be used for the reconstruction of an entire image series as a single inverse problem based on the spatial and temporal sparsity of the data. Moreover, the low-rank property inspired by the partially separable function model can be further utilized in accelerated dynamic MR imaging. In addition, we discussed several interesting trends including: 1) motion-corrected image reconstruction, which incorporates respiratory motion fields into image reconstruction for acceleration; 2) large-dimensional techniques exploiting higher dimensions such as motion and contrast sparsity in reconstruction; and 3) DL-based reconstruction. In conjunction with existing techniques such as parallel imaging, non-Cartesian trajectories and CS may further enhance the efficiency of real-time cardiac imaging at high spatiotemporal resolution.

REFERENCES

1. Lee DC, Markl M, Dall'Armellina E, et al. The growth and evolution of cardiovascular magnetic resonance: a 20-year history of the Society for Cardiovascular Magnetic Resonance (SCMR) annual scientific sessions. J Cardiovasc Magn Reson 2018;20:8
2. Lanzer P, Botvinick EH, Schiller NB, et al. Cardiac imaging using gated magnetic resonance. Radiology 1984;150:121-127
3. Frahm J, Voit D, Uecker M. Real-time magnetic resonance imaging: radial gradient-echo sequences with nonlinear inverse reconstruction. Invest Radiol 2019;54:757-766
4. Nayak KS, Lim Y, Campbell-Washburn AE, Steeden J. Real-time magnetic resonance imaging. J Magn Reson Imaging 2020
5. Dietz B, Fallone BG, Wachowicz K. Nomenclature for real-time magnetic resonance imaging. Magn Reson Med 2019;81:1483-1484
6. Sodickson DK, Manning WJ. Simultaneous acquisition of spatial harmonics (SMASH): fast imaging with radiofrequency coil arrays. Magn Reson Med 1997;38:591-603
7. Pruessmann KP, Weiger M, Scheidegger MB, Boesiger P. SENSE: sensitivity encoding for fast MRI. Magn Reson Med 1999;42:952-962
8. Griswold MA, Jakob PM, Heidemann RM, et al. Generalized autocalibrating partially parallel acquisitions (GRAPPA). Magn Reson Med 2002;47:1202-1210
9. Pruessmann KP, Weiger M, Boesiger P. Sensitivity encoded cardiac MRI. J Cardiovasc Magn Reson 2001;3:1-9
10. Kellman P, Epstein FH, McVeigh ER. Adaptive sensitivity encoding incorporating temporal filtering (TSENSE). Magn Reson Med 2001;45:846-852

11. Breuer FA, Kellman P, Griswold MA, Jakob PM. Dynamic autocalibrated parallel imaging using temporal GRAPPA (TGRAPPA). Magn Reson Med 2005;53:981-985
12. Madore B, Glover GH, Pelc NJ. Unaliasing by fourier-encoding the overlaps using the temporal dimension (UNFOLD), applied to cardiac imaging and fMRI. Magn Reson Med 1999;42:813-828
13. Tsao J, Boesiger P, Pruessmann KP. k-t BLAST and k-t SENSE: dynamic MRI with high frame rate exploiting spatiotemporal correlations. Magn Reson Med 2003;50:1031-1042
14. Pedersen H, Kozerke S, Ringgaard S, Nehrke K, Kim WY. k-t PCA: temporally constrained k-t BLAST reconstruction using principal component analysis. Magn Reson Med 2009;62:706-716
15. Brummer ME, Moratal-Perez D, Hong CY, Pettigrew RI, Millet-Roig J, Dixon WT. Noquist: reduced field-of-view imaging by direct Fourier inversion. Magn Reson Med 2004;51:331-342
16. Malik SJ, Schmitz S, O'Regan D, Larkman DJ, Hajnal JV. x-f Choice: reconstruction of undersampled dynamic MRI by data-driven alias rejection applied to contrast-enhanced angiography. Magn Reson Med 2006;56:811-823
17. Huang F, Akao J, Vijayakumar S, Duensing GR, Limkeman M. k-t GRAPPA: a k-space implementation for dynamic MRI with high reduction factor. Magn Reson Med 2005;54:1172-1184
18. Tsao J, Kozerke S. MRI temporal acceleration techniques. J Magn Reson Imaging 2012;36:543-560
19. Lauterbur PC. Image formation by induced local interactions: examples employing nuclear magnetic resonance. Nature 1973;242:190-191
20. Ahn CB, Kim JH, Cho ZH. High-speed spiral-scan echo planar NMR imaging-I. IEEE Trans Med Imaging 1986;5:2-7
21. Uecker M, Lai P, Murphy MJ, et al. ESPIRiT--an eigenvalue approach to autocalibrating parallel MRI: where SENSE meets GRAPPA. Magn Reson Med 2014;71:990-1001
22. Seiberlich N, Ehses P, Duerk J, Gilkeson R, Griswold M. Improved radial GRAPPA calibration for real-time free-breathing cardiac imaging. Magn Reson Med 2011;65:492-505
23. Seiberlich N, Lee G, Ehses P, Duerk JL, Gilkeson R, Griswold M. Improved temporal resolution in cardiac imaging using through-time spiral GRAPPA. Magn Reson Med 2011;66:1682-1688
24. Walsh DO, Gmitro AF, Marcellin MW. Adaptive reconstruction of phased array MR imagery. Magn Reson Med 2000;43:682-690
25. Pruessmann KP, Weiger M, Bornert P, Boesiger P. Advances in sensitivity encoding with arbitrary k-space trajectories. Magn Reson Med 2001;46:638-651
26. Ying L, Sheng J. Joint image reconstruction and sensitivity estimation in SENSE (JSENSE). Magn Reson Med 2007;57:1196-1202
27. Uecker M, Hohage T, Block KT, Frahm J. Image reconstruction by regularized nonlinear inversion--joint estimation of coil sensitivities and image content. Magn Reson Med 2008;60:674-682
28. Bakushinsky AB, Kokurin MY. Iterative methods for approximate solution of inverse problems. Mathematics and its applications. Springer Science & Business Media, 2005
29. Engl HW, Hanke M, Neubauer A. Regularization of inverse problems (Vol. 375). Springer Science & Business Media, 1996
30. Uecker M, Zhang S, Voit D, Karaus A, Merboldt KD, Frahm J. Real-time MRI at a resolution of 20 ms. NMR Biomed 2010;23:986-994
31. Wajer FTAW, Pruessmann KP. Major speedup of reconstruction for sensitivity encoding with arbitrary trajectories. In Proc Intl Soc Mag Res Med, 2001:767
32. Uecker M, Zhang S, Frahm J. Nonlinear inverse reconstruction for real-time MRI of the human heart using undersampled radial FLASH. Magn Reson Med 2010;63:1456-1462
33. Zhang S, Uecker M, Voit D, Merboldt KD, Frahm J. Real-time cardiovascular magnetic resonance at high temporal resolution: radial FLASH with nonlinear inverse reconstruction. J Cardiovasc Magn Reson 2010;12:39
34. Unterberg-Buchwald C, Ritter CO, Reupke V, et al. Targeted endomyocardial biopsy guided by real-time cardiovascular magnetic resonance. J Cardiovasc Magn Reson 2017;19:45
35. Campbell-Washburn AE, Tavallaei MA, Pop M, et al. Real-time MRI guidance of cardiac interventions. J Magn Reson Imaging 2017;46:935-950
36. Backhaus SJ, Lange T, George EF, et al. Exercise stress real-time cardiac magnetic resonance imaging for noninvasive characterization of heart failure with preserved ejection fraction: the HFpEF-Stress trial. Circulation 2021;143:1484-1498
37. Schaetz S, Voit D, Frahm J, Uecker M. Accelerated computing in magnetic resonance imaging: real-time imaging using nonlinear inverse reconstruction. Comput Math Methods Med 2017;2017:3527269
38. Block KT, Uecker M, Frahm J. Model-based iterative reconstruction for radial fast spin-echo MRI. IEEE Trans Med Imaging 2009;28:1759-1769
39. Fessler JA. Model-based image reconstruction for MRI. IEEE Signal Process Mag 2010;27:81-89
40. Tan Z, Roeloffs V, Voit D, et al. Model-based reconstruction

for real-time phase-contrast flow MRI: improved spatiotemporal accuracy. Magn Reson Med 2017;77:1082-1093
41. Wang X, Roeloffs V, Klosowski J, et al. Model-based T1 mapping with sparsity constraints using single-shot inversion-recovery radial FLASH. Magn Reson Med 2018;79:730-740
42. Wang X, Tan Z, Scholand N, Roeloffs V, Uecker M. Physics-based reconstruction methods for magnetic resonance imaging. Philos Trans A Math Phys Eng Sci 2021;379:20200196
43. Donoho DL. Compressed sensing. IEEE Trans Inf Theory 2006;52:1289-1306
44. Candès EJ, Romberg J, Tao T. Robust uncertainty principles: exact signal reconstruction from highly incomplete frequency information. IEEE Trans Inf Theory 2006;52:489-509
45. Lustig M, Donoho D, Pauly JM. Sparse MRI: the application of compressed sensing for rapid MR imaging. Magn Reson Med 2007;58:1182-1195
46. Block KT, Uecker M, Frahm J. Undersampled radial MRI with multiple coils. Iterative image reconstruction using a total variation constraint. Magn Reson Med 2007;57:1086-1098
47. Gamper U, Boesiger P, Kozerke S. Compressed sensing in dynamic MRI. Magn Reson Med 2008;59:365-373
48. Feng L, Benkert T, Block KT, Sodickson DK, Otazo R, Chandarana H. Compressed sensing for body MRI. J Magn Reson Imaging 2017;45:966-987
49. Liang D, Liu B, Wang J, Ying L. Accelerating SENSE using compressed sensing. Magn Reson Med 2009;62:1574-1584
50. Otazo R, Kim D, Axel L, Sodickson DK. Combination of compressed sensing and parallel imaging for highly accelerated first-pass cardiac perfusion MRI. Magn Reson Med 2010;64:767-776
51. Lustig M, Santos JM, Donoho DL, Pauly JM. k-t SPARSE: high frame rate dynamic MRI exploiting spatio-temporal sparsity. In Proceedings of the 13th Annual Meeting of ISMRM, 2006:2420
52. Usman M, Prieto C, Schaeffter T, Batchelor PG. k-t Group sparse: a method for accelerating dynamic MRI. Magn Reson Med 2011;66:1163-1176
53. Ting ST, Ding Y, Giri S, Jin N, Simonetti OP, Ahmad R. Sub-30 ms real-time, free-breathing cardiac imaging with SPIRiT. J Cardiovasc Magn Reson 2014;16:1-3
54. Ting ST, Ahmad R, Jin N, et al. Fast implementation for compressive recovery of highly accelerated cardiac cine MRI using the balanced sparse model. Magn Reson Med 2017;77:1505-1515
55. Ye JC. Compressed sensing MRI: a review from signal processing perspective. BMC Biomed Eng 2019;1:1-17
56. Feng L, Srichai MB, Lim RP, et al. Highly accelerated real-time cardiac cine MRI using k-t SPARSE-SENSE. Magn Reson Med 2013;70:64-74
57. Hager W, Zhang H. A new conjugate gradient method with guaranteed descent and an efficient line search. SIAM J Optim 2005;16:170-192
58. Daubechies I, Defrise M, De Mol C. An iterative thresholding algorithm for linear inverse problems with a sparsity constraint. Commun Pure Appl Math 2004;57:1413-1457
59. Beck A, Teboulle M. A fast iterative shrinkage-thresholding algorithm for linear inverse problems. SIAM J Imaging Sci 2009;2:183-202
60. Boyd S, Parikh N, Chu E, Peleato B, Eckstein J. Distributed optimization and statistical learning via the alternating direction method of multipliers. Found Trends Mach Learn 2011;3:1-122
61. Liu J, Rapin J, Chang TC, Lefebvre A, Zenge M, Mueller E, Nadar MS. Dynamic cardiac MRI reconstruction with weighted redundant Haar wavelets. In Proceedings of the 20th Annual Meeting of the ISMRM, 2012:4249
62. Qu X, Hou Y, Lam F, Guo D, Zhong J, Chen Z. Magnetic resonance image reconstruction from undersampled measurements using a patch-based nonlocal operator. Med Image Anal 2014;18:843-856
63. Aharon M, Elad M, Bruckstein A. K-SVD: an algorithm for designing overcomplete dictionaries for sparse representation. IEEE Trans Signal Process 2006;54:4311-4322
64. Ravishankar S, Bresler Y. MR image reconstruction from highly undersampled k-space data by dictionary learning. IEEE Trans Med Imaging 2011;30:1028-1041
65. Caballero J, Price AN, Rueckert D, Hajnal JV. Dictionary learning and time sparsity for dynamic MR data reconstruction. IEEE Trans Med Imaging 2014;33:979-994
66. Brinegar C, Wu YJ, Foley LM, et al. Real-time cardiac MRI without triggering, gating, or breath holding. Annu Int Conf IEEE Eng Med Biol Soc 2008;2008:3381-3384
67. Zhao B, Haldar JP, Brinegar C, Liang ZP. Low rank matrix recovery for real-time cardiac MRI. Proc IEEE Int Symp Biomed Imaging, 2010:996-999
68. Lingala SG, Hu Y, DiBella E, Jacob M. Accelerated dynamic MRI exploiting sparsity and low-rank structure: k-t SLR. IEEE Trans Med Imaging 2011;30:1042-1054
69. Zhao B, Haldar JP, Christodoulou AG, Liang ZP. Image reconstruction from highly undersampled (k, t)-space data with joint partial separability and sparsity constraints. IEEE Trans Med Imaging 2012;31:1809-1820
70. Liang ZP. Spatiotemporal imaging with partially separable functions. Proc IEEE Int Symp Biomed Imaging, 2007:988-991
71. Batchelor PG, Atkinson D, Irarrazaval P, Hill DL, Hajnal

J, Larkman D. Matrix description of general motion correction applied to multishot images. Magn Reson Med 2005;54:1273-1280
72. Hansen MS, Sorensen TS, Arai AE, Kellman P. Retrospective reconstruction of high temporal resolution cine images from real-time MRI using iterative motion correction. Magn Reson Med 2012;68:741-750
73. Xue H, Kellman P, LaRocca G, Arai AE, Hansen MS. High spatial and temporal resolution retrospective cine cardiovascular magnetic resonance from shortened free breathing real-time acquisitions. J Cardiovasc Magn Reson 2013; 15:1-15
74. Usman M, Atkinson D, Odille F, et al. Motion corrected compressed sensing for free-breathing dynamic cardiac MRI. Magn Reson Med 2013;70:504-516
75. Li H, Haltmeier M, Zhang S, Frahm J, Munk A. Aggregated motion estimation for real-time MRI reconstruction. Magn Reson Med 2014;72:1039-1048
76. Feng L, Grimm R, Block KT, et al. Golden-angle radial sparse parallel MRI: combination of compressed sensing, parallel imaging, and golden-angle radial sampling for fast and flexible dynamic volumetric MRI. Magn Reson Med 2014;72:707-717
77. Feng L, Axel L, Chandarana H, Block KT, Sodickson DK, Otazo R. XD-GRASP: golden-angle radial MRI with reconstruction of extra motion-state dimensions using compressed sensing. Magn Reson Med 2016;75:775-788
78. Poddar S, Jacob M. Dynamic MRI using smoothness regularization on manifolds (SToRM). IEEE Trans Med Imaging 2016;35:1106-1115
79. Christodoulou AG, Shaw JL, Nguyen C, et al. Magnetic resonance multitasking for motion-resolved quantitative cardiovascular imaging. Nat Biomed Eng 2018;2:215-226
80. Shaw JL, Yang Q, Zhou Z, et al. Free-breathing, non-ECG, continuous myocardial T1 mapping with cardiovascular magnetic resonance multitasking. Magn Reson Med 2019;81:2450-2463
81. Wang N, Gaddam S, Wang L, et al. Six-dimensional quantitative DCE MR multitasking of the entire abdomen: method and application to pancreatic ductal adenocarcinoma. Magn Reson Med 2020;84:928-948
82. Cheng JY, Hanneman K, Zhang T, et al. Comprehensive motion-compensated highly accelerated 4D flow MRI with ferumoxytol enhancement for pediatric congenital heart disease. J Magn Reson Imaging 2016;43:1355-1368
83. Cheng JY, Zhang T, Alley MT, et al. Comprehensive multi-dimensional MRI for the simultaneous assessment of cardiopulmonary anatomy and physiology. Sci Rep 2017;7:5330
84. Winkelmann S, Schaeffter T, Koehler T, Eggers H, Doessel O. An optimal radial profile order based on the golden ratio for time-resolved MRI. IEEE Trans Med Imaging 2007;26:68-76
85. Larson AC, White RD, Laub G, McVeigh ER, Li D, Simonetti OP. Self-gated cardiac cine MRI. Magn Reson Med 2004;51:93-102
86. Rosenzweig S, Scholand N, Holme HCM, Uecker M. Cardiac and respiratory self-gating in radial MRI using an adapted singular spectrum analysis (SSA-FARY). IEEE Trans Med Imaging 2020;39:3029-3041
87. Wang S, Su Z, Ying L, et al. Accelerating magnetic resonance imaging via deep learning. Proc IEEE Int Symp Biomed Imaging 2016;2016:514-517
88. Hammernik K, Klatzer T, Kobler E, et al. Learning a variational network for reconstruction of accelerated MRI data. Magn Reson Med 2018;79:3055-3071
89. Schlemper J, Caballero J, Hajnal JV, Price AN, Rueckert D. A deep cascade of convolutional neural networks for dynamic MR image reconstruction. IEEE Trans Med Imaging 2018;37:491-503
90. Aggarwal HK, Mani MP, Jacob M. MoDL: model-based deep learning architecture for inverse problems. IEEE Trans Med Imaging 2019;38:394-405
91. Luo G, Zhao N, Jiang W, Hui ES, Cao P. MRI reconstruction using deep Bayesian estimation. Magn Reson Med 2020;84:2246-2261
92. Knoll F, Hammernik K, Zhang C, et al. Deep-learning methods for parallel magnetic resonance imaging reconstruction: a survey of the current approaches, trends, and issues. IEEE Signal Process Mag 2020;37:128-140
93. He Z, Zhou P, Zhu H. Study of the interactivity between mercury and cellular system labeled with carboxymethyl chitosan-coated quantum dots and its application in a real-time in-situ detection of mercury. Spectrochim Acta A Mol Biomol Spectrosc 2015;139:179-183
94. Ke Z, Zhu Y, Liang D. Cascaded residual dense networks for dynamic MR imaging with edge-enhanced loss constraint. Investig Magn Reson Imaging 2020;24:214-222
95. Park SJ, Ahn CB. Blended-transfer learning for compressed-sensing cardiac CINE MRI. Investig Magn Reson Imaging 2021;25:10-22
96. Hauptmann A, Arridge S, Lucka F, Muthurangu V, Steeden JA. Real-time cardiovascular MR with spatio-temporal artifact suppression using deep learning-proof of concept in congenital heart disease. Magn Reson Med 2019;81:1143-1156
97. Wundrak S, Paul J, Ulrici J, et al. Golden ratio sparse MRI using tiny golden angles. Magn Reson Med 2016;75:2372-2378